Potential and support-dependent hydrogen evolution reaction activation energies on sulfur vacancies of MoS2 from GC-DFT

Nawras Abidi, Audrey Bonduelle-Skrzypczak, Stephan N. Steinmann

Graphical Abstract

Potential and Support-Dependent Hydrogen Evolution Reaction Activation Energies on Sulfur Vacancies of MoS_2 from GC-DFT

Nawras Abidi, Audrey Bonduelle-Skrzypczak, Stephan N. Steinmann

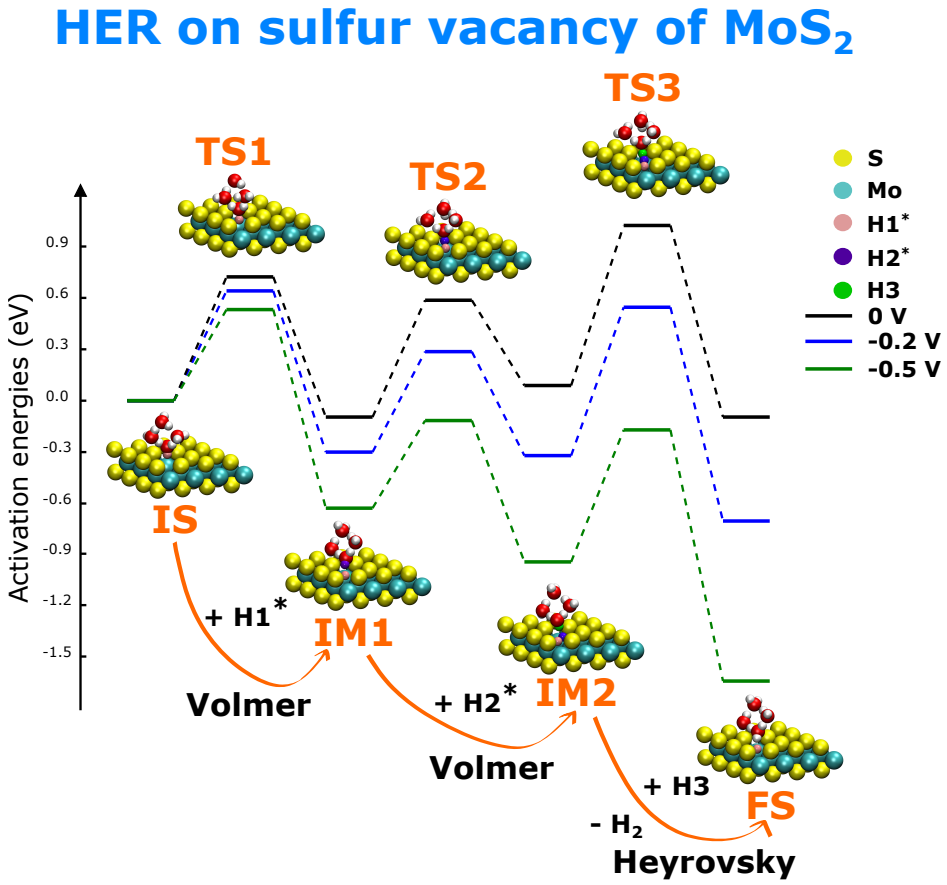

Highlights

Potential and Support-Dependent Hydrogen Evolution Reaction Activation Energies on Sulfur Vacancies of MoS_2 from GC-DFT

Nawras Abidi, Audrey Bonduelle-Skrzypczak, Stephan N. Steinmann

- Potential-dependent activation energies identify HER on S-vacancies of MoS_2 as a Volmer-Heyrovsky mechanism in presence of a spectator H*
- The defect density has little influence on the S-vacancy based HER kinetics
- Support and nanosheet size effects are found to be small, suggesting large specific surface area carbon supports are adequate for MoS_2

Potential and Support-Dependent Hydrogen Evolution Reaction Activation Energies on Sulfur Vacancies of MoS_2 from GC-DFT

Nawras Abidi[a], Audrey Bonduelle-Skrzypczak[b], Stephan N. Steinmann[a]

[a] *Univ Lyon, Ens de Lyon, CNRS UMR 5182, Laboratoire de Chimie, F69342, Lyon, France*
[b] *IFP Energies nouvelles, Rond-point de l'échangeur de Solaize, 69360, Solaize, France*

Abstract

We present a detailed mechanistic study of HER at the sulfur vacancy V_S of 2H-MoS_2. We evaluate the Volmer, Tafel, and Heyrovsky transition states for the different possible reaction steps, determining the activation energy as a function of the electrochemical potential via grand-canonical density functional theory. The results show that the Volmer and Heyrovsky steps depend on the electrochemical potential and the activation energies decrease for more negative potentials, while this is not the case for the Tafel step, for which the activation energy is constant. From the activation energies at -0.2 V vs SHE, it can be concluded that during HER on V_S a first hydrogen atom is adsorbed as a spectator via a Volmer step. Then, the catalytic cycle consists of a Volmer and a Heyrovsky step, with the latter being rate determining. In addition, we investigate for the first time the effect of a conductive support on the HER activity of these sulfur vacancies. Our results show that copper, gold and graphite supports have little effects on the activation energies of all steps. Hence, we conclude that cheap, acid-stable, high-surface area carbon supports are well suited for MoS_2-based HER catalysts.

Keywords: MoS_2 basal plane, Sulfur vacancies, Hydrogen evolution reaction, Grand-canonical DFT, Electrochemical potential, Activation energies, Support effect

1. Introduction

Hydrogen is expected to be one of the future clean energy vectors. Even though the electrochemical formation of H_2, the hydrogen evolution reaction (HER), is well studied for many decades, open questions still remain, as the detailed mechanism depends on the electrocatalyst and the reaction conditions.[1, 2] In acidic conditions, HER is, in general, a two-step process: The first step is the adsorption of protons from the acidic solution to form adsorbed H, denoted as H*. This step is the Volmer reaction:

$$H^+ + e^- \longrightarrow H^*(\text{Volmer reaction}) \tag{1}$$

The second step depends on the electrocatalyst and the current densities. It can be a Heyrovsky step:

$$H^* + H^+ + e^- \longrightarrow H_2(\text{Heyrovsky reaction}) \tag{2}$$

where a solvated proton reacts with H* to form H_2(g). Both the Volmer and the Heyrovsky reactions are "electrochemical" elementary steps, as they are formally coupled proton-electron transfers. Alternatively, H_2 can also be formed via a formally "chemical" step: the recombination of two H* to form H_2, known as the Tafel reaction:

$$H^* + H^* \longrightarrow H_2(\text{Tafel reaction}) \tag{3}$$

The rate of the overall reaction depends critically on the free energy of adsorption of the intermediate (H*) on the catalyst surface (ΔG_{H^*}), but the activation energies for the three elementary steps are responsible for the actual mechanism and the experimentally measured Tafel slopes (i.e., the relation between the overpotential and the current density).[3] According to the Sabatier principle (volcano diagram), ΔG_{H^*} should be close to 0 eV.[4]

Among the noble-metal free HER catalysts, transition metal dichalcogenides,[5, 6, 7, 8, 9] and in particular MoS_2,[10, 11, 12, 13, 14] are most promising for large-scale, low-cost applications in acidic medium, while phosphides are promising in alkaline solutions [15]. The development of these catalyst is one of the archetypal examples of a successful collaboration between computations and experiments.[4, 14] Several studies have shown that the basal plane and edges of the most stable MoS_2 polymorph (2H-MoS_2)[16] have contrasting electrocatalytic properties: the perfect 2H-MoS_2 basal plane is catalytically inert but the edges are highly active.[17]

To make 2H-MoS_2 catalytically more reactive, one can resort to methods of generating active sites by phase modifications,[18] doping [19, 20, 21, 22], or by exposing more edges [23, 24]. Furthermore, several studies have shown that point defects (and in particular the sulfur vacancies that have the lowest formation energy) also significantly affect the electrocatalytic properties of MoS_2.[25, 26, 27] The presence of these vacancy defects in MoS_2 effectively exposes the undercoordinated Mo atoms that act as active sites for the hydrogen evolution reaction (HER) as demonstrated by joint computational/experimental work. [28, 29, 30, 31, 32] These studies leave little doubt that such point defects are active sites for HER on MoS_2, even though the precise contribution between edge and basal plane activity is certainly highly dependent on the synthesis conditions and catalyst formulation. Experimentally, various efforts have been made to generate and precisely control the formation of sulfur defects on MoS_2 to catalyze HER, exploiting various techniques such as electrochemical desulfurization, chemical etching, oxygen/hydrogen plasma treatment, and high-temperature hydrogen annealing [16, 28, 33, 29, 31, 32, 34].

Since MoS_2 is a semiconductor, the HER activity of the basal plane is also limited by the electron transfer from the electrode to the catalyst.[35] Therefore, depositing MoS_2 nanosheets on a conductive support is an attractive strategy to improve the electron transfer kinetics and thus of the overall HER, in analogy to ideas in photocatalytic alkaline water splitting [36]. Furthermore, the support imparts mechanical stability to the catalyst and augments its dispersion, while limiting the size of the nanosheets during the synthesis. This is particularly beneficial for catalysts with high edge-site activities. The support can, however, also affect the electronic structure and coordination environment of MoS_2.[37, 38] Strong catalyst-support interactions have been found to reduce ΔG_{H*} and thus the support allows to tune the edge activity. Experimentally, a weakly interacting graphite support was demonstrated to lead to an increase in HER activity for the edges.[39] The high activity of Au nanostars encapsulated in a MoS_2 shell was rationalized by a slight improvement of the S-vacancy activity on a more strongly interacting Au support, but the the high electrical conductivity of the support and the high density of active sites might also contribute.[40]

While the use of the thermodynamics of HER, i.e., ΔG_{H*}, as a first approximation to the HER activity of MoS_2 was successful [41, 42, 43, 44], it does not provide insight into the reaction kinetics and the precise mechanisms involved. Activation energies ΔE_{act} are required to quantitatively

compute reaction rates and to elucidate the reaction mechanism. However, the computation of ΔE_{act} is not straightforward for electrocatalytic systems. Several methods have been developed to determine the transition states and activation energies, but no generally accepted, easily applicable scheme exists.[45] In our experience, grand canonical density functional theory (GC-DFT)[46, 47, 48] is the most versatile approach to determine potential-dependent activation energies. Previously, we have applied GC-DFT to elucidate the atomistic origin of the electrochemical promotion of catalysis.[49, 50, 51]

Using simplified models, i.e., that do not explicitly take the electrochemical potential into account, Li et al. [52] investigated the HER mechanism on MoS_2 with explicit consideration of the solvent effect. The results show that the solvent H_2O can significantly affect the barriers of HER . They proposed that HER at the MoS_2 (perfect) basal plane proceeds via the Volmer-Heyrovsky mechanism, and that the overall rate is determined by the Volmer step with an activation energy of 0.65 eV, which is at odds with the catalytic inertness of this surface. The HER mechanism at the defective basal plane of 2H-MoS_2, has only rarely been studied. Still using a simplified model (H_3O^+ is used as the reactant), Kong el al.[53] investigated the effects of sulfur vacancies distribution on the HER mechanism. Their computations suggest that HER proceeds via the Volmer-Heyrovsky mechanism with the Heyrovsky reaction as a rate-determined step (RDS) with an energy barrier of 0.8 eV on isolated defects. The study by Huang et al. [54] is the only one to date that has explicitly considered the effects of electrochemical potential on the activation energies of sulfur defects on MoS_2. Using grand-canonical potential kinetics, they conclude that the rate-determining step in both acidic and basic environments is the Volmer reaction, in which the second hydrogen is adsorbed from solution. This second hydrogen at the sulfur vacancy site is most active for the hydrogen evolution reaction. In acidic media, H_2 is generated via the Heyrovsky step with a barrier of 0.38 eV at -0.5 V. However, they used H_3O^+ as the reactant, which is likely[52] to be under-solvated by their implicit solvent.

Here, we investigate the kinetics of the HER on sulfur vacancies on the basal plane of 2H-MoS_2. Using GC-DFT we determine the activation energies governing the HER as a function of the electrochemical potential, using a hydronium ion (H_3O^+), microsolvated by three water molecules, giving $H_9O_4{}^+$. In addition, since in experimental setups a conductive support is necessary, we assess the effect of different supports (Au, Cu, and graphite)

compared to pure MoS_2 on these activation energies barriers.

2. Computational methods and models

2.1. Computational details

The computations were carried out relying on density functional theory with the Vienna ab initio simulation package (VASP) [55]. We adopted the PBE-dDsC [56, 57] density functional, which belongs to the family of the Generalized Gradient Approximation and is supplemented with a density-dependent dispersion correction.[58] The projector augmented wave method [59] is used to treat the ion–electron interaction. The electronic density was calculated with a 500 eV cutoff energy. Due to the size of the super cells, Γ point sampling of the Brillouin zone was found to be sufficient. The precision setting of VASP is set to "accurate". The convergence criterion for the self-consistency process is set to 10^{-5} eV for the optimization of the wave function. The maximum forces are converged to 0.025 eV/Å during the geometry optimization. The transition states (TS) were identified by the climbing image nudged-elastic band[60] and the dimer method [61]. Upon geometric convergence, a frequency analysis was performed to confirm the located TS and to verify the number of imaginary frequencies: one/two for as/symmetric slabs.

2.2. Energy evaluations

We are interested in evaluating the HER pathway and reaction kinetics of 2H-MoS_2. Therefore, we compute the hydrogen adsorption energy and the activation energy to determine the barrier for each step of the HER reaction.

For H_2 we use the following approximation for its free energy:

$$G_{H_2} = E_{H_2} - TS \tag{4}$$

where T is the room temperature (298.15 K) and S is the contribution of the rotational translational entropy at standard pressure.

To properly account for the electrochemical conditions at a given applied voltage, we use the grand canonical DFT approach. The number of electrons in the system is varied to probe the influence of the electrochemical potential. Counterions are included in the implicit solvation model via the linearized Poisson-Boltzmann equation to neutralize the system and provide a combined solvent-slab free energy.[62] This approach is implemented in

VASPsol[63], and we obtained a relationship between the grand canonical energy and the electrochemical potential fitted to an analytical formula that is a parabola for conductors.[64] An important parameter for the electrochemical computations is the iso-density value defining the solvent-solute interface. Following our previous studies [64], we have chosen 0.00025 $e^-/Å^{-3}$, which is one tenth of the default value and ensures the absence of implicit solvent between weakly bonded layers such as graphite and MoS_2.

The activation energy is calculated as a function of electrochemical potential by:

$$\Delta E_{act}(U) = E_{IS}(U) - E_{TS}(U) \tag{5}$$

Where $E_{IS}(U)$ and $E_{TS}(U)$ are the potential-dependent energies of the initial state and the transition state of the various steps obtained from the grand canonical energy as a function of the electrochemical potential.

As shown in Fig. S5, the potential of zero charge (corresponding to the neutral "conventional" surfaces) changes dramatically between the reactant ($H_9O_4^+ + e^-$) and the transition state, where the electron is no longer located on the surface, but is partially used to form the surface-H bond. Therefore, relying on the constant potential approach, i.e., GC-DFT, is key for these proton-electron transfer transition states. GC-DFT also allows to determine the charge transfer coefficient which determines the sensitivity of the activation energy on the applied potential, known from the empirical Buttler-Volmer equation. Indeed, in the GC-DFT framework, the charge transfer coefficient is simply obtained as the slope of the activation energy reported against the electrochemical potential. This allows an atomistic understanding of this otherwise empirical parameter.

2.3. Structural Models

The basal plane of MoS_2 consists of two hexagonal planes of sulfur (S) atoms and an intercalated hexagonal plane of molybdenum (Mo) atoms bonded to the S atoms. In the first part of our study, we work with the supercell of MoS_2 p(4×4) with three layers, where the bottom layer is fixed. A vacuum of about 30 Å is added in the z-direction (See Fig. 1a). A sulfur vacancy (V_s) is created by removing one sulfur atom. To model the proton/electron transfer reactions - Volmer and Heyrovsky reactions - we use a micro-solvated structure of the hydronium (H_3O^+) ion, where it is stabilized by three additional water molecules to form a $H_9O_4^+$ complex. This approach

is inspired by the work of Skulasson,[65] but in our hands the original $H_9O_4^+$ structure underwent a stabilizing rearrangement, forming the four-membered ring shown in Fig. 1a. For the Tafel step, since there is no electron transfer, only a surface slab and adsorbed hydrogens need to be included in the atomic model.

For assessing the support effect, we prepare a $Mo_{12}S_{24}$ triangular nanosheet from MoS_2 with reconstructed Mo-edges represented in Fig. 1b in order to avoid the strain of the support or MoS_2. Gronborg et al.[66] determined with scanning tunneling microscopy (STM) that MoS_2 nanosheets larger than 2 nm adopt a perfect triangular shape terminated by the Mo edges which is more stable than the S-edge under the sulfiding conditions of the synthesis. Then, we add the $H_9O_4^+$ structure based on the optimized geometries from the periodic MoS_2 surfaces. The nanosheet is positioned on different supports: Molybdenum disulfide (MoS_2) as a reference, gold (Au), copper (Cu) and graphite (C). (See Fig. 2) The gold support is chosen because of its use in previous experimental studies,[11, 67] copper as a cheaper metallic analogue and graphite is our model for conducting high-area carbon supports that are widely studied in the fuel-cell literature and used and on an industrial scale. Different positions of the nanosheet on the support were tested using ChemCat[68]: Top, Bridge, Hollow, fcc and hcp. The relative energy values are shown in Table S1. In all cases, the "top" position is the most stable.

To properly determine the workfunction of the various systems, we use symmetric slabs. Even though the use of asymmetric slabs has been proposed in the context of GC-DFT,[69] for the highly polar initial state and TS involving a proton, we have observed in Fig. S1 artifacts for the asymmetric potential dependent models. We suspect that these observations are due to the implicit solvent that is present on both surfaces, in contrast to ref. [69]. For the systems with support and only in the case of the first Volmer step (V^I), we realize plane symmetrization for the MoS_2 support and point symmetrization for Cu and Au. Graphite was not considered for these GC-DFT computations as the system is computationally excessively heavy. Our final symmetric slabs are made of five layers of the support, with the central layer frozen in its bulk position. (see Fig. S2).

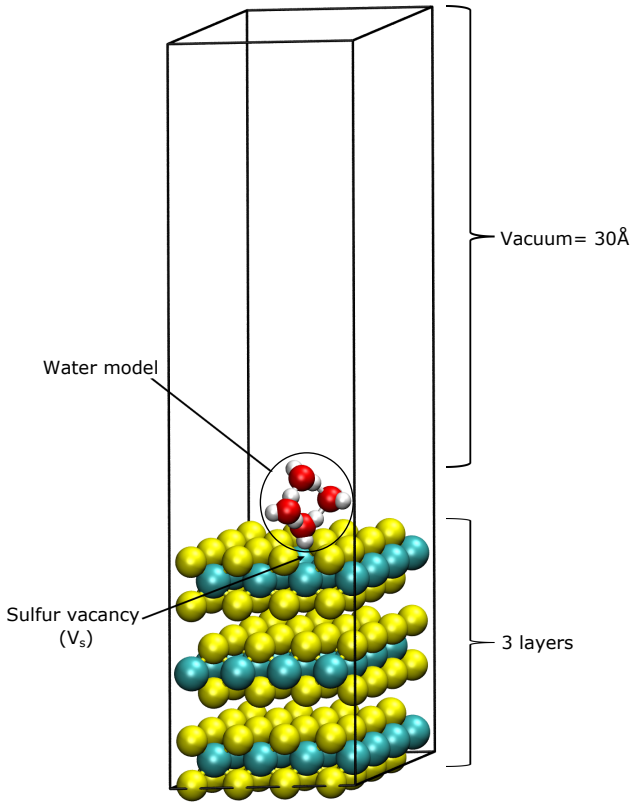

(a) MoS_2 basal plane

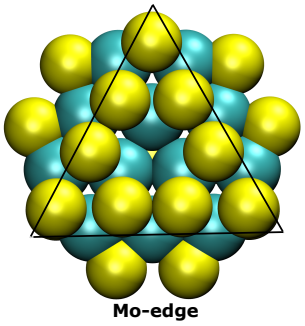

(b) MoS_2 nanosheet

Figure 1: (a) The structure of non-symmetric MoS_2 basal plane with the water model and the sulfur vacancy. (b) MoS_2 nanosheet with sulfur vacancy and triangular shape terminated by Mo edges. The color code for atoms is white for H; red for O; yellow for S and greenish for Mo.

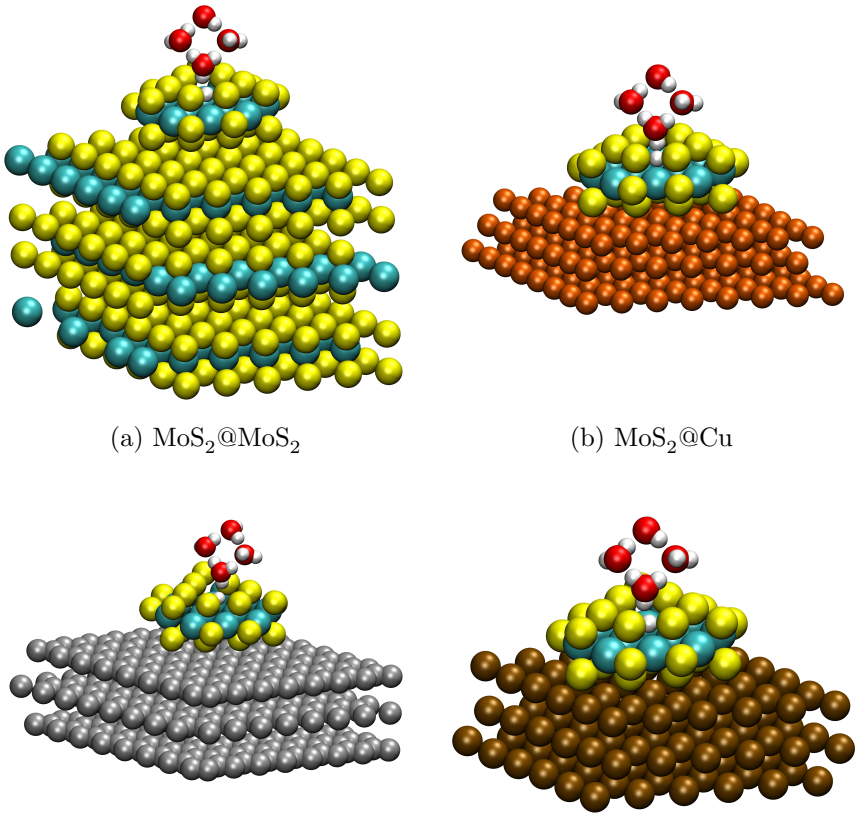

(a) MoS_2@MoS_2 (b) MoS_2@Cu

(c) MoS_2@C (d) MoS_2@Au

Figure 2: 3×3 MoS_2 nanosheet supported on molybdenum disulphide (a), copper (b), graphite (c) and gold (d). The structures presented correspond to the transition state of V^{II}. The color code for atoms is white for H; red for O; yellow for S, greenish for Mo, orange for Cu, grey for C and brown for Au.

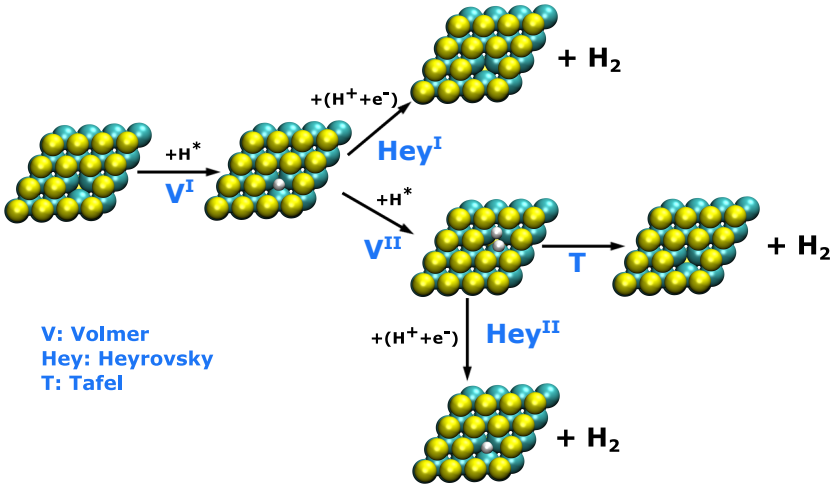

Figure 3: The different steps and the labels for the corresponding transition states of Volmer-Heyrovsky and Volmer-Tafel mechanisms to produce H_2 on the sulfur vacancy V_S. The color code for atoms is white for H; yellow for S and greenish for Mo.

3. Results and Discussion

3.1. HER mechanism on V_S

We start by the investigation of the mechanism of hydrogen production at the "isolated" sulfur vacancy (V_S). As shown in our previous study [64], V_S is an active site with hydrogen adsorption energy close to 0 eV (two hydrogen atoms can be adsorbed). Fig. 3 presents the different intermediates for the possible HER mechanisms. The results of hydrogen adsorption energies and activation energies at zero charge (i.e., without GC-DFT) are shown in Table S2 and Table S3, respectively.

By using GC-DFT, Fig. S3 shows the evolution of the adsorption energies of the two hydrogen atoms on V_S as a function of the electrochemical potential. We find that the production of H_2 is thermodynamically starting from -0.2 V vs SHE. Fig. 4 displays the optimized geometries of the different transition states for each step with the corresponding activation energies as a function of electrochemical potential. As shown, V^I, V^{II}, Hey^I and Hey^{II} depend strongly (0.34 eV/V) on the electrochemical potential, which is not the case for the formally chemical Tafel (T) step. This is in complete agreement with previous studies suggesting that Volmer and Heyrovsky are electrochemical steps while T is a chemical reaction.[54]

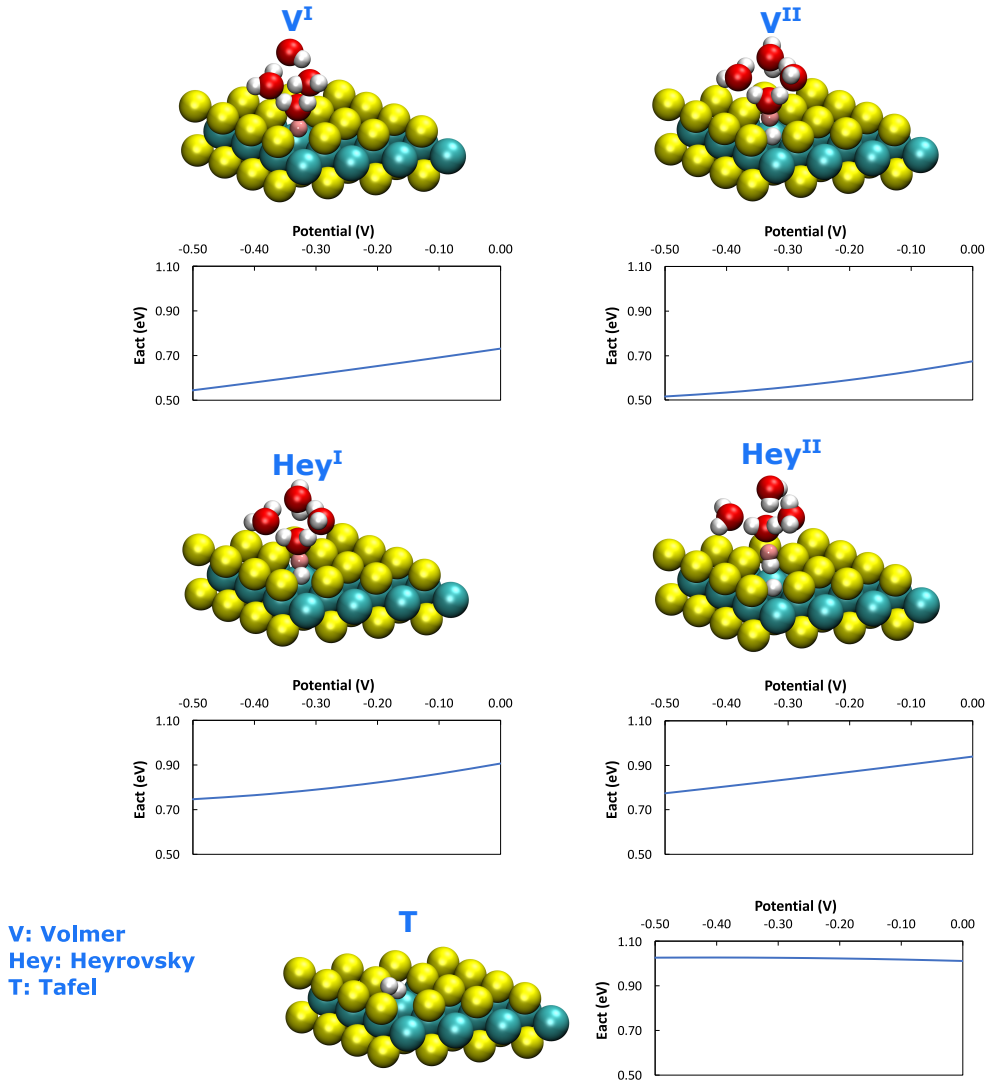

Figure 4: The structure of the different transition states and the variation of their activation energies as function of the electrochemical potential. The color code for atoms is white for H; pink for H coming from the water model; yellow for S and greenish for Mo.

As can be seen in Fig. 4, the hydrogen atom is adsorbed from the solution with a barrier of 0.54 eV at -0.5 V. This value can be compared to the corresponding activation energy of Huang et al.[54] which is much smaller (0.07 eV). Compared to our model, they used a smaller p(3 × 3) MoS_2 surface (instead of p(4 × 4) herein) and H_3O^+ as the proton source (instead of $H_9O_4{}^+$). Fig. S4 shows the variation of the activation energy of V_I as a function of electrochemical potential for p(4 × 4), our surface, and p(3 × 3) used by Huang et al.. We find that at a given electrochemical potential, the activation energy is lower by 0.05 eV at -0.2 V with p(4 × 4) than with p(3 × 3). Hence, this is not the origin of the difference between our barrier and the previous report. However, due to insufficiencies of the implicit solvent model, the proton is much less stabilised in H_3O^+ compared with $H_9O_4{}^+$. This greater stability of the initial species explains the increase in the barrier and is in line with a previous study comparing H_3O^+ and $H_5O_2{}^+$ as proton sources.[52]

To identify the HER pathway, we compare the activation energies of the different steps at -0.2 V vs SHE, which is close to the onset potential. The first step is V^I, the detachment of the hydrogen atom from H_3O^+ to be adsorbed onto the sulfur vacancy with ΔE_{act} of 0.65 eV. Then, H^* on V_s can interact with the solution proton to produce H_2 via the Hey^{II} reaction with a barrier of 0.82 eV. These results indicate that the first adsorbed H is not easily desorbed to generate H_2 because the sulfur vacancy has a strong adsorption energy for H^*. Therefore, before desorption of H_2, another H^+ plus e^- pair moves to the sulfur vacancy corresponding to V^{II} with a ΔE_{act} of 0.59 eV. Subsequently, H_2 is produced by Hey^{II}, the reaction of H^* with one electron and proton, or the combination with the second H^* (T). ΔE_{act} for Hey^{II} and T are 0.87 eV and 1.02 eV, respectively. Thus, Tafel step has a higher activation energy compared to Hey^{II}. Therefore, the HER occurs on the sulfur vacancy mainly via catalytic cycles between V^{II} and Hey^{II}. The Hey^{II} reaction is found to be the rate-determining step (RDS), as it has the highest barrier energy. Overall, these barriers are in good agreement with a reaction occurring at room temperature: According to the Eyring equation, it corresponds to a turn-over frequency of 0.2 per second.

3.2. The support effect

One of the strategies to improve the electrocatalytic water splitting activity of non-metallic catalysts such as MoS_2 is to enhance the charge transfer from the conductive support to the catalyst surfaces.[70] Here, we investigate

for the first time the effect of different supports on the activation energies of the elementary reactions for the release of H_2 on sulfur vacancies, including explicitly the electrochemical potential for one of the representative reactions. The corresponding structures are depicted in Fig. 2.

Identifying the transition states on all the supports has been a very tedious task, and despite significant efforts we have not been able to identify the transition state of Hey^{II} for any of them, so we exclude it from the following discussion. Fig. 5 shows the activation energies of V^I, V^{II}, Hey^I and T without considering the electrochemical potential. We find that the activation energies for V^I, V^{II} and Hey^I barely depend on the supports, implying that the type of support has no effect on the activation energy. The only notable difference is the Tafel step, where the copper support increases the activation energy by 0.26 eV. As detailed in section S4 of the Supporting Information, various tests were performed related to the nanosheet size, the deposition of a periodic surface of MoS_2 on the support instead of a nanosheet, and the defect density. The final result was always the same: the activation energies obtained are very close to those in Fig. 5. As a proxy for the electronic structure, we have analyzed the Hirshfeld atomic charges and their redistribution from the initial state to the TS, see Fig. S8 and S9. According to our analysis (see also the discussion in section S5), the atomic charges change only little as a function of the support and nanosheet vs. periodic MoS_2 layer. We conclude that there is a very small interaction between the MoS_2 nanosheet and the different supports and that neither the size of the nanosheet nor the number of (isolated) sulfur vacancies can contribute to the reduction of the barrier energies for the V^I step. Therefore, we conclude that for the release of H_2 with MoS_2 as electrocatalyst, MoS_2 support, gold or graphite give the same energy barrier. However, copper is to be avoided for this type of reaction.

Given that the potentials of zero charge vary by up to 1 V between the initial and transition states (see Fig. S5), we have also assessed the effect of the electrochemical potential on the activation energy for a typical electrochemical process. We have chosen V^I as a representative transition state, which also was computationally well behaved. Hence, we have symmetrized the corresponding systems (see section 2.3), except the graphite supported one which turned out to be computationally intractable. The GC-DFT results are depicted in Fig. 6, where the strong dependence of the activation energy on the electrochemical potential (and thus non-negligible, but support in-dependent) charge-transfer coefficient) is retrieved. We first note that the

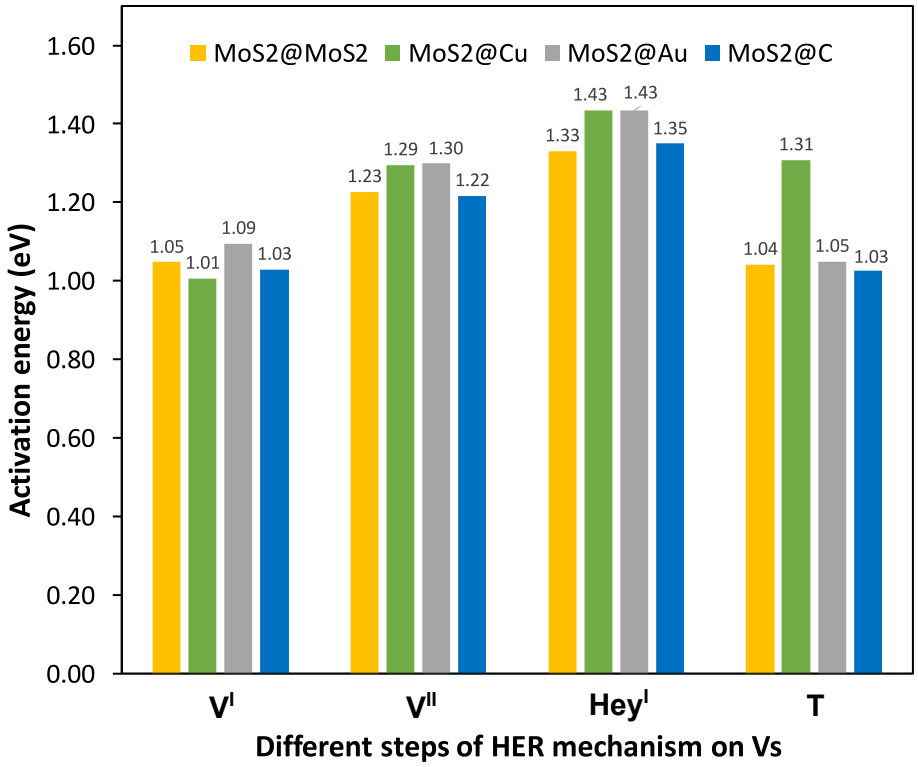

Figure 5: Comparison between the activation energies of HER mechanism steps on MoS_2 nanosheet with the different type of supports at zero charge, i.e., using canonical DFT, not GC-DFT. The colors used: yellow, green, grey and blue are for the supports MoS_2, copper, gold and graphite, respectively.

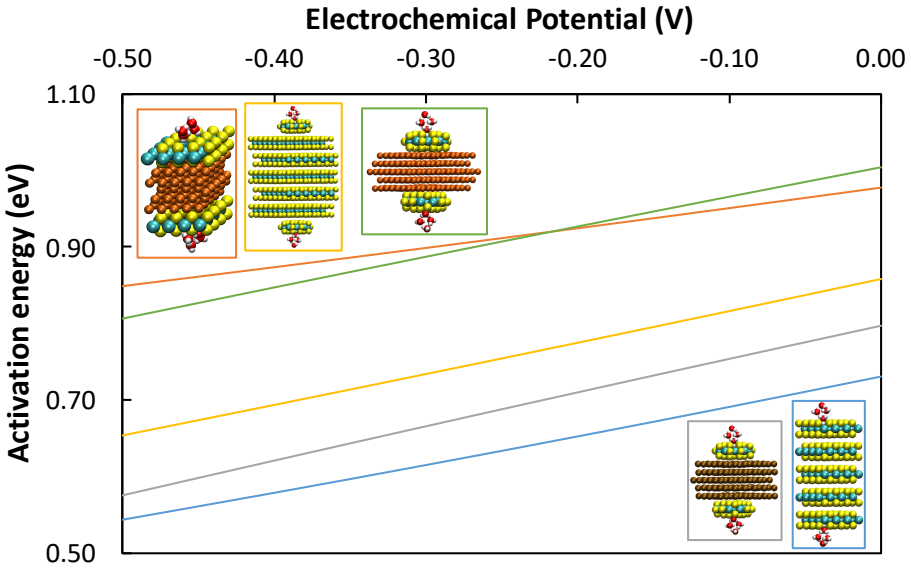

Figure 6: Variation of the activation energy as function of the electrochemical potential. The yellow, green and grey curves are for MoS_2 nanosheet supported on MoS_2, copper and gold respectively. The blue curve is the periodic MoS_2 surface and the orange color is for periodic MoS_2 monolayer supported on Cu.

nanosheet model supported on MoS_2 and the periodic MoS_2 surface give similar results (within ∼0.1 eV) and the nanosheet supported on Au is right in the middle and hence close to the pure MoS_2 systems. For the Cu support, we find that the barrier energy increases for nanosheets or periodic surfaces of MoS_2, confirming that this type of support should be avoided. Based on these results, we suggest that a conductive (graphitic) carbon support (from the non-symmetric results) is more advantageous compared to expensive gold electrodes.

From these various computations and models, we can draw several conclusions: First, the increasing or decreasing of the defect density has little effect on the HER activity: Starting from a rather high (1 per p(3×3) unit cell (or 1.3×10^{13} per cm^2) defect density down to 1 per p(6×6) unit cell (or 3.1×10^{12} per cm^2) leads to equivalent activation energies (see Fig. S4 and S7). Second, only symmetric slabs ensure reliable conclusions on the impact of the support. This originates in the difference in workfunction between the "occupied" and "unoccupied" support surfaces. The most telling example is MoS_2@Cu: For an asymmetric system, the surface bound electrons, that

depend on the electrochemical potential, are shared among the "bare" and the "covered" surface. Hence, the overall workfunction is roughly the average, which impacts the energetics for reactions where the polarity changes dramatically, such as the Volmer step, where one moves from $H_3O^+ + e^-$ to $H^* + H_2O$. Third, in the systems studied herein, the charge-transfer is "weak", in the sense that it is not due to a chemical interaction, but just due to the equalization of the Fermi-levels of the different materials. However, in electrocatalysis the Fermi-level is determined by the electrode potential. Hence, the GC-DFT framework reveals that the weak charge-transfer has no significant impact on electrocatalysts. This is best seen for the "size" effect (small nanosheet vs. monolayer) where the change in electronic structure is small enough to be largely counteracted by the electrode potential. However, "stronger" modifications, such as doping [71, 72] and defect engineering [73, 74] has, of course, a role to play even in electrocatalysis.

4. Conclusion

We have investigated the kinetics of HER over sulfur vacancies on the MoS_2 basal plane. We have identified the activation energies of the five plausible elementary steps (two consecutive Volmer steps, one Tafel step and two Heyrovsky steps) as a function of the electrochemical potential. In agreement with expectations based on the change of polarity between the reactant and the transition state, the Tafel step is a purely chemical step at the potentials of interest and does, therefore, not depend significantly on the electrochemical potential. The Volmer and Heyrovsky barriers, are, in contrast, dependent on the electrochemical potential, with a slope of about 0.34 eV/V. We then investigated means to tune the HER kinetics over these defects via support effects, size effects (nanosheet vs. periodic surface) and defect density. While in the absence of the electrochemical potential such a tuning seems possible, taking the electrochemical potential explicitly into account "washes out" these effects. In other words, the "intrinsic" activity of the sulfur vacancy is retrieved essentially independently on the size of the sheets, the defect density and the support. Hence, small nanosheets on a high surface area carbon support are likely to be an optimal choice, as it simply increases the number of active sites on a geometrical area basis and should, therefore, lead to a high geometrical current density.

Author Contributions

Nawras Abidi: Investigation, Writing - Original Draft
Audrey Bonduelle-Skrzypczak: Writing - Review
Stephan N. Steinmann: Supervision, Conceptualization, Resources, Writing - Review & Editing

Conflicts of interest

There are no conflicts to declare

Acknowledgements

This work was financially supported by Région Auvergne Rhône-Alpes through the project Pack Ambition Recherche 2018 MoSHi. We are very grateful to IFP Energies nouvelles for supporting the MoSHy project (N^o 1801167601) and to the IFP Energies nouvelles team, Mona Marie Obadia and Quentin Cacciuttolo, for fruitful discussions.The authors thank the SYSPROD project and AXELERA Pôle de Compétitivité for financial support (PSMN Data Center).

Supporting Information

The supplementary material contains computational details and additional Figures and Tables. Coordinates and DFT raw data is freely available on NOMAD-lab: https://dx.doi.org/10.17172/NOMAD/2022.09.07-1.

References

[1] Y. Zheng, Y. Jiao, M. Jaroniec, S. Z. Qiao, Advancing the electrochemistry of the hydrogen-evolution reaction through combining experiment and theory, Angewandte Chemie International Edition 54 (1) (2015) 52–65.

[2] A. Lasia, Mechanism and kinetics of the hydrogen evolution reaction, international journal of hydrogen energy 44 (36) (2019) 19484–19518.

[3] T. Shinagawa, A. T. Garcia-Esparza, K. Takanabe, Insight on Tafel slopes from a microkinetic analysis of aqueous electrocatalysis for energy conversion, Sci Rep 5 (1) (2015) 13801.

[4] Z. W. Seh, J. Kibsgaard, C. F. Dickens, I. Chorkendorff, J. K. Nørskov, T. F. Jaramillo, Combining theory and experiment in electrocatalysis: Insights into materials design, Science 355 (6321) (2017).

[5] D. Kong, J. J. Cha, H. Wang, H. R. Lee, Y. Cui, First-row transition metal dichalcogenide catalysts for hydrogen evolution reaction, Energy & Environmental Science 6 (12) (2013) 3553–3558.

[6] D. Voiry, H. Yamaguchi, J. Li, R. Silva, D. C. Alves, T. Fujita, M. Chen, T. Asefa, V. B. Shenoy, G. Eda, et al., Enhanced catalytic activity in strained chemically exfoliated ws 2 nanosheets for hydrogen evolution, Nature materials 12 (9) (2013) 850–855.

[7] C. Tsai, K. Chan, F. Abild-Pedersen, J. K. Nørskov, Active edge sites in mose 2 and wse 2 catalysts for the hydrogen evolution reaction: a density functional study, Physical Chemistry Chemical Physics 16 (26) (2014) 13156–13164.

[8] M. A. Lukowski, A. S. Daniel, C. R. English, F. Meng, A. Forticaux, R. J. Hamers, S. Jin, Highly active hydrogen evolution catalysis from metallic ws 2 nanosheets, Energy & Environmental Science 7 (8) (2014) 2608–2613.

[9] M. S. Faber, S. Jin, Earth-abundant inorganic electrocatalysts and their nanostructures for energy conversion applications, Energy & Environmental Science 7 (11) (2014) 3519–3542.

[10] B. Hinnemann, P. G. Moses, J. Bonde, K. P. Jørgensen, J. H. Nielsen, S. Horch, I. Chorkendorff, J. K. Nørskov, Biomimetic hydrogen evolution: Mos2 nanoparticles as catalyst for hydrogen evolution, Journal of the American Chemical Society 127 (15) (2005) 5308–5309.

[11] T. F. Jaramillo, K. P. Jørgensen, J. Bonde, J. H. Nielsen, S. Horch, I. Chorkendorff, Identification of active edge sites for electrochemical h2 evolution from mos2 nanocatalysts, science 317 (5834) (2007) 100–102.

[12] Y. Li, H. Wang, L. Xie, Y. Liang, G. Hong, H. Dai, Mos2 nanoparticles grown on graphene: an advanced catalyst for the hydrogen evolution reaction, Journal of the American Chemical Society 133 (19) (2011) 7296–7299.

[13] J. Kibsgaard, Z. Chen, B. N. Reinecke, T. F. Jaramillo, Engineering the surface structure of MoS_2 to preferentially expose active edge sites for electrocatalysis, Nature materials 11 (11) (2012) 963–969.

[14] J. D. Benck, T. R. Hellstern, J. Kibsgaard, P. Chakthranont, T. F. Jaramillo, Catalyzing the hydrogen evolution reaction (HER) with molybdenum sulfide nanomaterials, ACS Catalysis 4 (11) (2014) 3957–3971.

[15] X. Guo, M. Li, L. Qiu, F. Tian, L. He, S. Geng, Y. Liu, Y. Song, W. Yang, Y. Yu, Engineering electron redistribution of bimetallic phosphates with CeO2 enables high-performance overall water splitting, Chemical Engineering Journal 453 (2023) 139796.

[16] M. Chhowalla, H. S. Shin, G. Eda, L.-J. Li, K. P. Loh, H. Zhang, The chemistry of two-dimensional layered transition metal dichalcogenide nanosheets, Nature chemistry 5 (4) (2013) 263–275.

[17] C. Tsai, K. Chan, J. K. Nørskov, F. Abild-Pedersen, Theoretical insights into the hydrogen evolution activity of layered transition metal dichalcogenides, Surface Science 640 (2015) 133–140.

[18] D. Voiry, M. Salehi, R. Silva, T. Fujita, M. Chen, T. Asefa, V. B. Shenoy, G. Eda, M. Chhowalla, Conducting mos2 nanosheets as catalysts for hydrogen evolution reaction, Nano letters 13 (12) (2013) 6222–6227.

[19] P. Liu, J. Zhu, J. Zhang, P. Xi, K. Tao, D. Gao, D. Xue, P dopants triggered new basal plane active sites and enlarged interlayer spacing in mos2 nanosheets toward electrocatalytic hydrogen evolution, ACS Energy Letters 2 (4) (2017) 745–752.

[20] Y. Shi, Y. Zhou, D.-R. Yang, W.-X. Xu, C. Wang, F.-B. Wang, J.-J. Xu, X.-H. Xia, H.-Y. Chen, Energy level engineering of mos2 by transition-metal doping for accelerating hydrogen evolution reaction, Journal of the American Chemical Society 139 (43) (2017) 15479–15485.

[21] J. Pető, T. Ollár, P. Vancsó, Z. I. Popov, G. Z. Magda, G. Dobrik, C. Hwang, P. B. Sorokin, L. Tapasztó, Spontaneous doping of the basal plane of mos2 single layers through oxygen substitution under ambient conditions, Nature chemistry 10 (12) (2018) 1246–1251.

[22] X. Zhang, F. Zhou, S. Zhang, Y. Liang, R. Wang, Engineering mos2 basal planes for hydrogen evolution via synergistic ruthenium doping and nanocarbon hybridization, Advanced Science 6 (10) (2019) 1900090.

[23] D. Voiry, A. Mohite, M. Chhowalla, Phase engineering of transition metal dichalcogenides, Chemical Society Reviews 44 (9) (2015) 2702–2712.

[24] J. Hu, B. Huang, C. Zhang, Z. Wang, Y. An, D. Zhou, H. Lin, M. K. Leung, S. Yang, Engineering stepped edge surface structures of mos 2 sheet stacks to accelerate the hydrogen evolution reaction, Energy & Environmental Science 10 (2) (2017) 593–603.

[25] Y. Yin, J. Han, Y. Zhang, X. Zhang, P. Xu, Q. Yuan, L. Samad, X. Wang, Y. Wang, Z. Zhang, et al., Contributions of phase, sulfur vacancies, and edges to the hydrogen evolution reaction catalytic activity of porous molybdenum disulfide nanosheets, Journal of the American Chemical Society 138 (25) (2016) 7965–7972.

[26] Y. Ouyang, C. Ling, Q. Chen, Z. Wang, L. Shi, J. Wang, Activating inert basal planes of mos2 for hydrogen evolution reaction through the formation of different intrinsic defects, Chemistry of Materials 28 (12) (2016) 4390–4396.

[27] G. Li, D. Zhang, Q. Qiao, Y. Yu, D. Peterson, A. Zafar, R. Kumar, S. Curtarolo, F. Hunte, S. Shannon, et al., All the catalytic active sites of mos2 for hydrogen evolution, Journal of the American Chemical Society 138 (51) (2016) 16632–16638.

[28] H. Li, C. Tsai, A. L. Koh, L. Cai, A. W. Contryman, A. H. Fragapane, J. Zhao, H. S. Han, H. C. Manoharan, F. Abild-Pedersen, et al., Activating and optimizing mos2 basal planes for hydrogen evolution through the formation of strained sulphur vacancies, Nature materials 15 (1) (2016) 48–53.

[29] G. Ye, Y. Gong, J. Lin, B. Li, Y. He, S. T. Pantelides, W. Zhou, R. Vajtai, P. M. Ajayan, Defects engineered monolayer mos2 for improved hydrogen evolution reaction, Nano letters 16 (2) (2016) 1097–1103.

[30] C. Tsai, H. Li, S. Park, J. Park, H. S. Han, J. K. Nørskov, X. Zheng, F. Abild-Pedersen, Electrochemical generation of sulfur vacancies in the

basal plane of mos2 for hydrogen evolution, Nature communications 8 (1) (2017) 1–8.

[31] L. Li, Z. Qin, L. Ries, S. Hong, T. Michel, J. Yang, C. Salameh, M. Bechelany, P. Miele, D. Kaplan, et al., Role of sulfur vacancies and undercoordinated mo regions in mos2 nanosheets toward the evolution of hydrogen, ACS nano 13 (6) (2019) 6824–6834.

[32] J. Yang, Y. Wang, M. J. Lagos, V. Manichev, R. Fullon, X. Song, D. Voiry, S. Chakraborty, W. Zhang, P. E. Batson, et al., Single atomic vacancy catalysis, ACS nano 13 (9) (2019) 9958–9964.

[33] C.-C. Cheng, A.-Y. Lu, C.-C. Tseng, X. Yang, M. N. Hedhili, M.-C. Chen, K.-H. Wei, L.-J. Li, Activating basal-plane catalytic activity of two-dimensional mos2 monolayer with remote hydrogen plasma, Nano Energy 30 (2016) 846–852.

[34] X. Wang, Y. Zhang, H. Si, Q. Zhang, J. Wu, L. Gao, X. Wei, Y. Sun, Q. Liao, Z. Zhang, et al., Single-atom vacancy defect to trigger high-efficiency hydrogen evolution of mos2, Journal of the American Chemical Society 142 (9) (2020) 4298–4308.

[35] Y. Yu, S. Y. Huang, Y. Li, S. N. Steinmann, W. Yang, L. Cao, Layer-dependent electrocatalysis of MoS2 for hydrogen evolution, Nano Letters 14 (2) (2014) 553–558.

[36] X. Zhang, C. Zhu, L. Qiu, M. Gao, F. Tian, Y. Liu, W. Yang, Y. Yu, Concentrating photoelectrons on sulfur sites of ZnxCd1–xS to active H–OH bond of absorbed water boosts photocatalytic hydrogen generation, Surfaces and Interfaces 34 (2022) 102312.

[37] C. Tsai, F. Abild-Pedersen, J. K. Nørskov, Tuning the MoS2 Edge-Site Activity for Hydrogen Evolution via Support Interactions, Nano Lett. 14 (3) (2014) 1381–1387.

[38] P. Wang, L. Wan, Y. Lin, B. Wang, Mos2 supported cos2 on carbon cloth as a high-performance electrode for hydrogen evolution reaction, International Journal of Hydrogen Energy 44 (31) (2019) 16566–16574.

[39] Q. Xu, Y. Liu, H. Jiang, Y. Hu, H. Liu, C. Li, Unsaturated sulfur edge engineering of strongly coupled mos2 nanosheet–carbon macroporous

hybrid catalyst for enhanced hydrogen generation, Advanced Energy Materials 9 (2) (2019) 1802553.

[40] R. Bar-Ziv, P. Ranjan, A. Lavie, A. Jain, S. Garai, A. Bar Hen, R. Popovitz-Biro, R. Tenne, R. Arenal, A. Ramasubramaniam, et al., Au-mos2 hybrids as hydrogen evolution electrocatalysts, ACS Applied Energy Materials 2 (8) (2019) 6043–6050.

[41] C. G. Morales-Guio, L.-A. Stern, X. Hu, Nanostructured hydrotreating catalysts for electrochemical hydrogen evolution, Chemical Society Reviews 43 (18) (2014) 6555–6569.

[42] X. Gao, Y. Zhou, Y. Tan, B. Yang, Z. Cheng, Z. Shen, J. Jia, Mo isolated single atoms on s, n-codoped carbon as efficient catalyst for hydrogen evolution reaction: A theoretical evaluation, Applied Surface Science 473 (2019) 770–776.

[43] Y. J. Sa, S. O. Park, G. Y. Jung, T. J. Shin, H. Y. Jeong, S. K. Kwak, S. H. Joo, Heterogeneous co–n/c electrocatalysts with controlled cobalt site densities for the hydrogen evolution reaction: structure–activity correlations and kinetic insights, ACS Catalysis 9 (1) (2018) 83–97.

[44] T. Sun, J. Wang, X. Chi, Y. Lin, Z. Chen, X. Ling, C. Qiu, Y. Xu, L. Song, W. Chen, C. Su, Engineering the Electronic Structure of MoS2 Nanorods by N and Mn Dopants for Ultra-Efficient Hydrogen Production, ACS Catalysis 8 (2018) 7585–7592.

[45] N. Abidi, S. N. Steinmann, How are transition states modelled in heterogeneous electrocatalysis?, Current Opinion in Electrochemistry (2022) 100940.

[46] H.-F. Wang, Z.-P. Liu, Formic Acid Oxidation at Pt/H2O Interface from Periodic DFT Calculations Integrated with a Continuum Solvation Model, J. Phys. Chem. C 113 (40) (2009) 17502.

[47] R. Jinnouchi, A. B. Anderson, Electronic structure calculations of liquid-solid interfaces: Combination of density functional theory and modified Poisson-Boltzmann theory, Phys. Rev. B 77 (24) (2008) 245417.

[48] K. Letchworth-Weaver, T. A. Arias, Joint density functional theory of the electrode-electrolyte interface: Application to fixed electrode potentials, interfacial capacitances, and potentials of zero charge, Phys. Rev. B 86 (7) (2012) 075140.

[49] Y. M. Hajar, L. Treps, C. Michel, E. A. Baranova, S. N. Steinmann, Theoretical insight into the origin of the electrochemical promotion of ethylene oxidation on ruthenium oxide, Catalysis Science and Technology 9 (21) (2019) 5915–5926. doi:10.1039/c9cy01421g.

[50] C. Panaritis, C. Michel, M. Couillard, E. A. Baranova, S. N. Steinmann, Elucidating the role of electrochemical polarization on the selectivity of the CO2 hydrogenation reaction over Ru, Electrochimica Acta 350 (2020) 136405.

[51] C. Panaritis, Y. M. Hajar, L. Treps, C. Michel, E. A. Baranova, S. N. Steinmann, Demystifying the Atomistic Origin of the Electric Field Effect on Methane Oxidation, J. Phys. Chem. Lett. 11 (17) (2020) 6976–6981.

[52] W. Li, G. Liu, J. Li, Y. Wang, L. Ricardez-Sandoval, Y. Zhang, Z. Zhang, Hydrogen evolution reaction mechanism on 2h-mos2 electrocatalyst, Applied Surface Science 498 (2019) 143869.

[53] C. Kong, Y.-X. Han, L.-j. Hou, P.-J. Yan, The distribution effect of sulfur vacancy in 2h–mos2 monolayer on its h2 generation mechanism from density functional theory, International Journal of Hydrogen Energy 47 (1) (2022) 242–249.

[54] Y. Huang, R. J. Nielsen, W. A. Goddard III, Reaction mechanism for the hydrogen evolution reaction on the basal plane sulfur vacancy site of mos2 using grand canonical potential kinetics, Journal of the American Chemical Society 140 (48) (2018) 16773–16782.

[55] G. Kresse, J. Furthmüller, Efficient iterative schemes for ab initio total-energy calculations using a plane-wave basis set, Physical review B 54 (16) (1996) 11169.

[56] J. P. Perdew, K. Burke, M. Ernzerhof, Generalized gradient approximation made simple, Physical review letters 77 (18) (1996) 3865.

[57] S. N. Steinmann, C. Corminboeuf, Comprehensive benchmarking of a density-dependent dispersion correction, Journal of chemical theory and computation 7 (11) (2011) 3567–3577.

[58] S. N. Steinmann, P. Sautet, C. Michel, Solvation free energies for periodic surfaces: comparison of implicit and explicit solvation models, Physical Chemistry Chemical Physics 18 (46) (2016) 31850–31861.

[59] G. Kresse, D. Joubert, From ultrasoft pseudopotentials to the projector augmented-wave method, Physical review b 59 (3) (1999) 1758.

[60] G. Henkelman, B. P. Uberuaga, H. Jónsson, A climbing image nudged elastic band method for finding saddle points and minimum energy paths, The Journal of chemical physics 113 (22) (2000) 9901–9904.

[61] G. Henkelman, H. Jónsson, A dimer method for finding saddle points on high dimensional potential surfaces using only first derivatives, The Journal of chemical physics 111 (15) (1999) 7010–7022.

[62] N. Abidi, K. R. G. Lim, Z. W. Seh, S. N. Steinmann, Atomistic modeling of electrocatalysis: Are we there yet?, Wiley Interdisciplinary Reviews: Computational Molecular Science 11 (3) (2021) e1499.

[63] K. Mathew, V. S. C. Kolluru, S. Mula, S. N. Steinmann, R. G. Hennig, Implicit self-consistent electrolyte model in plane-wave density-functional theory, J. Chem. Phys. 151 (23) (2019) 234101.

[64] N. Abidi, A. Bonduelle-Skrzypczak, S. N. Steinmann, Revisiting the active sites at the mos2/h2o interface via grand-canonical dft: The role of water dissociation, ACS applied materials & interfaces 12 (28) (2020) 31401–31410.

[65] M. Van den Bossche, E. Skúlason, C. Rose-Petruck, H. Jónsson, Assessment of Constant-Potential Implicit Solvation Calculations of Electrochemical Energy Barriers for H2 Evolution on Pt, J. Phys. Chem. C 123 (7) (2019) 4116–4124.

[66] S. S. Grønborg, N. Salazar, A. Bruix, J. Rodríguez-Fernández, S. D. Thomsen, B. Hammer, J. V. Lauritsen, Visualizing hydrogen-induced reshaping and edge activation in mos2 and co-promoted mos2 catalyst clusters, Nature communications 9 (1) (2018) 1–11.

[67] J. Zhang, J. Wu, H. Guo, W. Chen, J. Yuan, U. Martinez, G. Gupta, A. Mohite, P. M. Ajayan, J. Lou, Unveiling active sites for the hydrogen evolution reaction on monolayer mos2, Advanced Materials 29 (42) (2017) 1701955.

[68] C. Martí, S. Blanck, R. Staub, S. Loehlé, C. Michel, S. N. Steinmann, DockOnSurf: A Python Code for the High-Throughput Screening of Flexible Molecules Adsorbed on Surfaces, J. Chem. Inf. Model. 61 (7) (2021) 3386–3396.

[69] C. D. Taylor, S. A. Wasileski, J.-S. Filhol, M. Neurock, First principles reaction modeling of the electrochemical interface: Consideration and calculation of a tunable surface potential from atomic and electronic structure, Physical Review B 73 (16) (2006) 165402.

[70] J. Zhang, Q. Zhang, X. Feng, Support and interface effects in water-splitting electrocatalysts, Advanced Materials 31 (31) (2019) 1808167.

[71] S. Chen, Y. Pan, Noble metal interlayer-doping enhances the catalytic activity of 2h–mos2 from first-principles investigations, International Journal of Hydrogen Energy 46 (40) (2021) 21040–21049.

[72] X. Chen, J. Sun, J. Guan, J. Ji, M. Zhou, L. Meng, M. Chen, W. Zhou, Y. Liu, X. Zhang, Enhanced hydrogen evolution reaction performance of mos2 by dual metal atoms doping, International Journal of Hydrogen Energy 47 (55) (2022) 23191–23200.

[73] W. Chen, L. Sun, Q. Li, L. Huo, H. Zhao, Defect-rich mos2/r-go hybrid via microwave-assisted solvothermal process for efficient electrocatalytic hydrogen evolution, International Journal of Hydrogen Energy 45 (43) (2020) 22459–22468.

[74] S. Saleem, M. Salman, S. Ali, Y. Ling, M. Khan, Electrocatalytic hydrogen evolution reaction on sulfur-deficient mos2 nanostructures, International Journal of Hydrogen Energy 47 (12) (2022) 7713–7723.